IEEE Photonics Journal
An IEEE Photonics Society Publication

Open Access

Radially Polarized Orbital Angular Momentum Beam Emitter Based on Shallow-Ridge Silicon Microring Cavity

Volume 6, Number 3, June 2014

Rui Li
Xue Feng
Dengke Zhang
Kaiyu Cui
Fang Liu
Yidong Huang, Member, IEEE

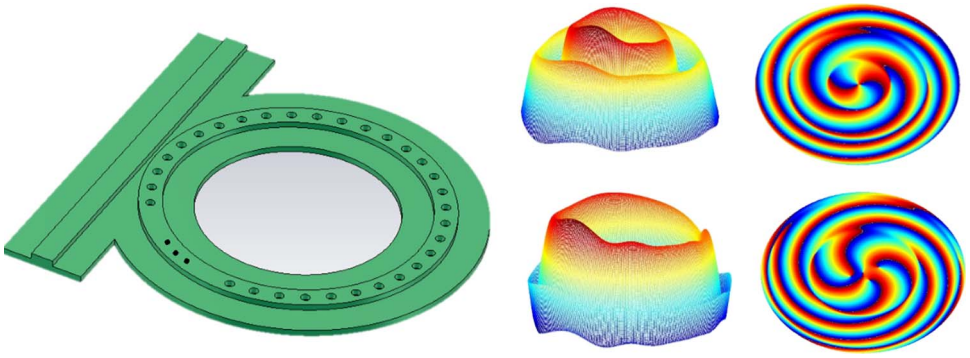

DOI: 10.1109/JPHOT.2014.2321757
1943-0655

IEEE photonics SOCIETY

IEEE

Radially Polarized Orbital Angular Momentum Beam Emitter Based on Shallow-Ridge Silicon Microring Cavity

Rui Li, Xue Feng, Dengke Zhang, Kaiyu Cui, Fang Liu, and Yidong Huang, *Member, IEEE*

Department of Electronic Engineering, Tsinghua National Laboratory for Information Science and Technology, Tsinghua University, Beijing 100084, China

DOI: 10.1109/JPHOT.2014.2321757

Manuscript received April 1, 2014; revised April 24, 2014; accepted April 24, 2014. Date of current version May 14, 2014. This work was supported by the National Basic Research Program of China under Grant 2011CBA00608, Grant 2011CBA00303, Grant 2011CB301803, and Grant 2010CB327405; by the National Natural Science Foundation of China under Grant 61307068, Grant 61036010, Grant 61036011, and Grant 61321004; and by the Opened Fund of the State Key Laboratory on Integrated Optoelectronics, China, under Grant IOSKL2013KF09. Corresponding author: X. Feng (e-mail: x-feng@tsinghua.edu.cn).

Abstract: Radially polarized orbital angular momentum (OAM) beams could be applied in optical manipulation and optical microscopy. An integrated OAM beam emitter with radially polarized radiation is proposed on shallow-ridge silicon microring with azimuthally distributed gratings etched on top of the ring waveguide. Two key structural parameters, the number of grating elements, and the dimension of each grating element are optimized by considering both the OAM order purity (C_p) and the total radiation efficiency (η_{all}). With elaborate design, $C_p = \sim 98\%$, $\eta_{all} = \sim 49\%$ are achieved by simulations, and the calculated energy ratio between the far-field radially and azimuthally polarized component is more than 11 dB, which indicates that the radially polarized component is predominant in the radiated electromagnetic field.

Index Terms: Optical orbital angular momentum (OAM), radial polarization, shallow-ridge microring.

1. Introduction

Light beams with helical phase fronts and spiral flow of electromagnetic energy have attracted much interest since they could carry orbital angular momentum (OAM) [1]–[3]. OAM beam could be applied in optical tweezers and spanners [4]–[6], optical microscopy [7], [8], quantum and wireless communications [9]–[11], etc. Conventionally, the OAM beam could be generated through some bulk optical components such as holograms [12], [13], spiral phase plates [14]. In recent two years, integrated OAM beam emitters are considered to take advantage of compactness, reliability and potential to be applied in photonic integrated circuit (PIC) [15]–[17]. In [16], an OAM beam emitter based on a silicon microring and azimuthally distributed gratings is proposed and demonstrated. Such an OAM beam emitter is considered to be applied in integrated OAM switches or modulators and micromanipulation of particles [16]. In our previous work [17], an integrated OAM beam emitter based on ring cavity and download waveguides (each including an arc-shaped section next to the ring and gratings near the ring's center) is proposed as encoder for wireless optical interconnects on silicon chip. For the application of optical communication, the polarization of the emitted beam is not

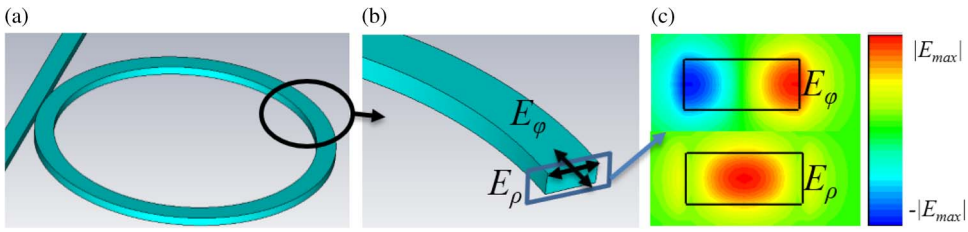

Fig. 1. (a) The schematic of a silicon microring. (b) The cross section of the bent waveguide of the microring E_φ is the azimuthal electric field, and E_ρ is the radial electric field. (c) The calculated azimuthal and radial electric field distribution of the cross section.

a critical factor. But considering the applications of optical manipulation and microscopy, it is desired to generate radially polarized light beams. Since a light beam with radial polarization can be focused to a spot size that is dramatically smaller than that with linear polarization, the longitudinal electric field component oscillates at the incident beam frequency and exists only near the focus [18]–[20]. Thus, it can be applied to guide or trap particles [21], [22] and increase the resolution in optical microscopy [23]. If radially polarized OAM beams could be generated on a chip, the advantages of OAM beam and radial polarization as well as photonic integration could be obtained for optical manipulation and microscopy. However, in both [16] and [17], the generated OAM beams are predominantly azimuthally polarized.

In this work, a radially polarized OAM beam emitter based on shallow-ridge silicon microring is proposed. Azimuthally distributed gratings are adopted to generate OAM beam and each grating element is a hole etched on top of the waveguide to scatter radially polarized light. A simple dipole model, which is similar to that used in [24], is applied to calculate the emitted electromagnetic field. The number (q) of grating elements and the radius (r) of the grating element are optimized by considering both the OAM order purity (C_p) and the total radiation efficiency (η_{all}). With the optimized parameters of $q = 270$ and $r = 50$ nm, the cross-coupling coefficient is calculated as 0.87 and finally, $C_p = \sim 98\%$, $\eta_{all} = \sim 49\%$ are achieved by simulations. Moreover, the calculated energy ratio between the far-field radially and azimuthally polarized component is more than 11 dB.

2. Scheme and Principle

It has been demonstrated that the whispering gallery modes (WGMs) of a ring cavity can carry high order OAM [25]. By introducing some azimuthally distributed gratings or download waveguides, the confined WGMs in the ring cavity can be extracted into radiative mode and OAM beam is generated in succession [16], [17]. In [16], the fundamental mode with quasi-transverse electric (TE) polarization in the silicon waveguide is used to excite quasi-TE WGM mode in the ring cavity. Fig. 1(a) is the schematic of a silicon microring cavity with the same dimension as [16]. The radius of the ring is 3.9 μm, the width and height of waveguide are 500 nm and 220 nm, respectively. The silicon waveguide is surrounded by silica and the calculated effective index is around 2.5. Fig. 1(b) shows the cross section of the ring waveguide in which the directions of the azimuthal electric field E_φ and radial electric field E_ρ are indicated. Fig. 1(c) shows the calculated electric field distribution of the cross section, which is obtained by three-dimensional finite difference time domain (3D-FDTD) method. The wavelength is 1550 nm, which is one of resonant peaks for the calculated microring. It can be seen that the electric field on the sidewall and on top of the waveguide are dominant with azimuthal and radial polarization, respectively. Thus, as shown in [16], the scattered light beam would be predominantly in azimuthal direction if gratings are fabricated on the sidewall of the waveguide. On the contrary, in order to obtain radially polarized light beam, gratings should be placed on top of waveguide to scatter electric field with radial polarization.

To obtain OAM beam with radial polarization, the schematic of our proposed emitter is shown in Fig. 2(a). There are one ring cavity and one bus waveguide. Both the ring and the bus waveguide

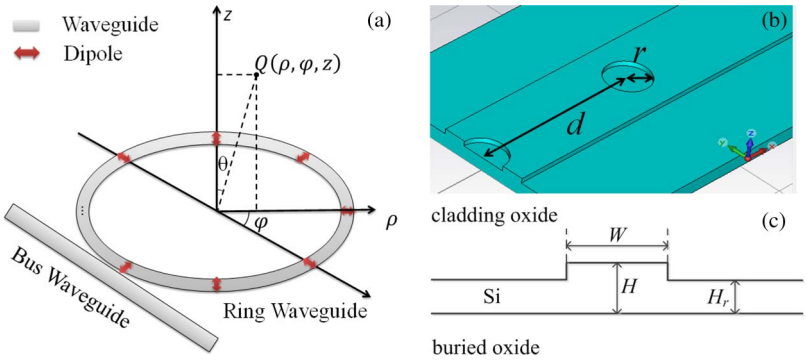

Fig. 2. Schematic diagram of (a) dipole model of our proposed OAM beam emitter, (b) gratings on top of the waveguide, (c) shallow-ridge waveguide.

are shallow-ridge waveguides. As shown in Fig. 2(b), there are some holes on top of the ring waveguide that serve as the grating elements. All holes are identical and equidistantly distributed along the ring. The hole depth is considered as same as the ridge height of the waveguide. The radius of each hole and the grating constant are denoted as r and d, respectively. The reason of adopting shallow-ridge waveguide is that the propagation loss can be rather low (0.278 dB/cm, [26]). Furthermore, the waveguide and the gratings can be etched at the same time since the hole depth is equal to the ridge height of the waveguide. Thus, such design is convenient for fabrication. The radius of the ring is set as $R = 49$ μm which is the minimum value to assure a low bending loss ($\sim$0.1 dB/cm [27]). The gap between the ring waveguide and the bus waveguide would be meticulously designed to achieve critical coupling. Fig. 2(c) is the schematic of the shallow-ridge waveguide. The waveguide has a width of $W = 750$ nm, a slab region thickness of $H_r = 170$ nm, and a ridge thickness of $H = 220$ nm which is corresponding to the thickness of the top silicon layer of a Silicon-on-Insulator (SOI) wafer. These conditions could assure the single mode operation within wavelength range around1550 nm for the shallow-ridge waveguide [27]. The effective index (n_{eff}) of the shallow-ridge waveguide is 2.72, which is calculated by the finite element method (FEM).

According to the result in [16], the order of radiated OAM beam (l) satisfies

$$l = p - gq \tag{1}$$

where p is the WGM order in the ring, q is the number of grating elements around the resonator, and g is the diffraction order which is an integer and could be calculated as:

$$(n_{eff} - 1) \cdot \frac{2\pi R}{q\lambda} < g < (n_{eff} + 1) \cdot \frac{2\pi R}{q\lambda}. \tag{2}$$

For the ring radius of 49 μm, at the resonance wavelength of 1550 nm, the WGM order p is 540, thus the number of grating elements q can be chosen as $540/t$ $(t = 1, 2, 3 \ldots)$ to make sure that the $l = 0$ (corresponding to plane-wave), so the maximum value of q is 540. Then g is an integer between $0.63t$ and $1.37t$ with $n_{eff} = 2.72$ according to Eq. (2). Thus, g is related to q and the impact of g factor will be discussed in the following session. It should be mentioned that the operating wavelength could be arbitrary with a proper radius of microring. For a fabricated device, q will remain the same while p can be changed by tuning the operation wavelength according to cavity resonances. For C-band (1530–1565 nm), $l = -4 \sim 4$ is considered and the relation of operating wavelength λ versus p and l is shown in Table 1. Here $q = 540$ is taken and the g factor is calculated as $g = 1$.

3. Simulations and Results

In order to verify the performance of our proposed OAM beam emitter, some numerical simulations have been carried on. The most straightforward way is utilizing 3D-FDTD simulation. However, the

TABLE 1

The operating wavelength λ versus the number of grating elements p and the order of radiated OAM beam l

λ(nm)	1561.6	1558.7	1555.8	1552.9	1550	1547.1	1544.3	1541.4	1538.6
p	536	537	538	539	540	541	542	543	544
l	-4	-3	-2	-1	0	1	2	3	4

time and space complexity would significantly increase as the radius of the ring increases. According to our experience, the 3D-FDTD simulation is almost unrealizable when the radius of the microring is more than 30 μm due to limitations in computational resources. In [24], a theoretical model based on a simple dipole representation of grating scattering has been proposed to derive the near- and far-zone emission characteristics of the azimuthally distributed grating-based OAM beam emitters. And the calculations using this model agree well with the experimental results in previous work [16]. This model is also adopted to calculate the far-field intensity profile of the microdisk laser emission [28]. Thus, we also employ the dipole model instead of 3D-FDTD calculation to simulate our proposed OAM beam emitter. In [24], azimuthal polarized dipole radiation is applied since grating elements are on the sidewall of the ring waveguide and scattered light is mainly azimuthally polarized. Different from that, the radially polarized dipole is adopted in our calculation since the gratings on top of the waveguide would mainly scatter the radially polarized electric field.

The model is established in a cylindrical coordinate (ρ, φ, z), where ρ and z are the polar radius and distance from ring plane. All dipoles are assumed with a time dependent term of $e^{-j\omega t}$, and they are located uniformly along the resonator circumference with $\rho = R$ on the emitter plane $(z = 0)$, as illustrated in Fig. 2(a).

For an arbitrary observation point denoted as Q (ρ, φ, z) located in the upper hemisphere [$z > 0$, see Fig. 2(a)], the field results from the interference of the radiation of all dipoles could be expressed as:

$$E_l(\rho,\varphi,z) = \frac{1}{4\pi\varepsilon_0 R^3} \cdot \sum_{m=1}^{q} \left\{ P_m \cdot e^{j\nu r_m} \cdot e^{jl\varphi_m} \cdot \left[\left(\frac{\nu^2}{r_m} - j\frac{\nu}{r_m^2} - \frac{1}{r_m^3} \right) (\hat{r}_m \times \hat{\rho}_m) \times \hat{r}_m - \left(j\frac{2\nu}{r_m^2} + \frac{2}{r_m^3} \right) (\hat{r}_m \cdot \hat{\rho}_m) \cdot \hat{r}_m \right] \right\} \tag{3}$$

where $\nu = 2\pi/\lambda$, λ is the vacuum wavelength, r_m is the distance between Q and the mth dipole point $S_m(R, \varphi_m, 0)$, P_m is the intensity of mth dipole, and $\hat{r}_m$ is the unit vector in the direction of S_mQ, pointing from S_m.

Since $q = 540/t$, q is firstly considered as maximum value 540 $(t = 1)$ which is equal to WGM order at the operating wavelength $(\lambda = 1550$ nm$)$ and the intensity of all the dipoles are considered as equal. According to Eqs. (1) and (2), the diffraction order g and WGM order of the microring p could be calculated as $g = 1$ and $p = q + l$ so that the phase difference of adjacent dipoles will be $2l\pi/q$ and the phase of the mth dipole will be $2n(m-1)\pi/q$ when the phase of the first dipole is set as 0. Thus different orders of OAM beam could be generated by tuning the phases of dipoles in this model (which is equivalent of switching WGM order p). Fig. 3 shows the calculated transversal phase distributions of the far-field of OAM orders varied from 0 to 3. Here, λ is selected according to l, as shown in Table 1.

In Fig. 3, the amplitude of each dipole radiation is considered as identical. However, for a practical device, each grating element would introduce attenuation during the light propagation. If the energy radiation efficiency of each grating (denoted as η) is taken into account, due to the scattering of gratings, the intensity of mth grating element should be:

$$P_m = P_0 \cdot (1-\eta)^{0.5m} \tag{4}$$

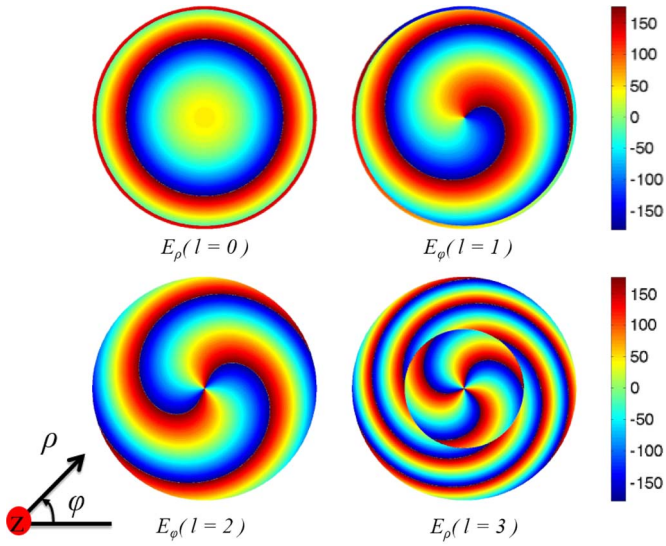

Fig. 3. Calculated transversal phase distribution of the far-field radiation.

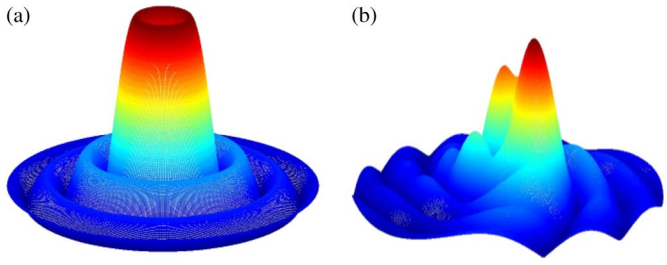

Fig. 4. Calculated far-field intensity distribution of azimuthal component with (a) $\eta = 0$, (b) $\eta = 0.01$.

where P_0 is the intensity of the first grating element. The intensity of each dipole radiation is not identical any more so that the generated OAM beam would be deteriorated. As a concrete example, the azimuthal components of far-field intensity distribution with $\eta = 0$ and $\eta = 0.01$ $(l = -2)$ are calculated and shown in Fig. 4.

It can be seen that the far-field intensity varies with φ for the same ρ in Fig. 4(b) while it is constant in Fig. 4(a). It indicates that the OAM beam deforms with nonzero η. To investigate the impact of η on the quality of OAM beam, here we introduce a parameter C_p to represent the OAM order purity. To calculate the OAM purity of the emitted beam, the different orders of OAM beams calculated by dipole model with the maximum value of the number of grating elements $(q = 540)$ and $\eta = 0$ are considered as a set of basis and the corresponding electric field is denoted as $E_l(\varphi, \theta)$ with order l, where both the radial and the azimuthal components are included in E_l. The OAM order purity C_p is defined as the overlap of the calculated electric field of OAM beam and the electric field of the basis which could be calculated as:

$$C_p = \frac{\int\int E(\varphi,\theta)\cdot E_l^*(\varphi,\theta) sin\theta d\varphi d\theta}{\sqrt{\int E(\varphi,\theta)\cdot E^*(\varphi,\theta) sin\theta d\varphi d\theta \int E_l(\varphi,\theta)\cdot E_l^*(\varphi,\theta) sin\theta d\varphi d\theta}} \tag{5}$$

where $E(\varphi, \theta)$ is the electric field of OAM beam calculated with a given η. Our defined OAM order purity has the similar physical meaning to that in [29], where the helical LG modes form a complete set of basis. Additionally, it should be mentioned that the integration is calculated along the spherical surface since the propagation phase front is spherical. For a practical device, only part of

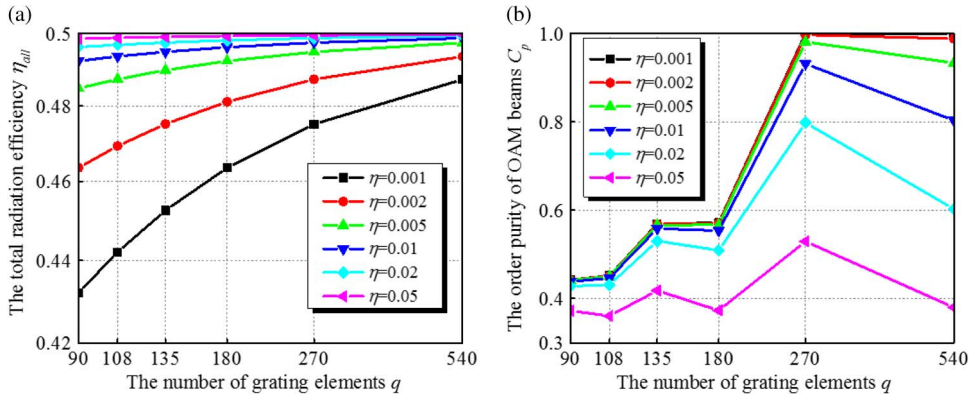

Fig. 5. (a) The total radiative efficiency η_{all} and (b) the purity C_p of the OAM beams versus the number of grating elements q and the radiation efficiency of single grating element η.

the radiation can be collected by the detecting system so that the half-angle of the maximum cone of light that can enter or exit the lens should be considered. According to the N.A. of ∼0.9 which is at most for air medium, the half-angle is calculated as ∼60°. Thus, $\theta = 0° \sim 60°$ and $\varphi = 0° \sim 360°$ is considered in our calculation. The overlap between the OAM beam basis $E_l\ (\varphi, \theta)$ with $l = -4 \sim 4$ are calculated. $C_p = 1$ for OAM beams with same l and $C_p < 1e-3$ for OAM beams with different l, which are proved that the selected OAM beam basis are orthogonal to each other.

Besides the order purity, the total radiation efficiency (denoted as η_{all}) of the OAM beam emitter is also an important characteristic for OAM beam emitter. For the ring cavity, η_{all} could be calculated as:

$$\eta_{all} = \frac{\eta}{1 - (1-\eta)\cdot(1-\alpha)^2} \tag{6}$$

here α is the propagation loss of the waveguide between two adjacent grating elements. The detail of the deduction is shown in appendix.

For designing the OAM beam emitter, our goal is to achieve both high order purity and high total radiation efficiency, and they have different relation to the structural parameters especially with q and η. So we calculate the variations of order purity and total radiation efficiency versus different q and η. In our calculation, q is set as $540/t$, $t = 1 \sim 6$, while η is set as $0.001 \sim 0.05$. Fig. 5 shows the results of the purity C_p and the total efficiency η_{all} of the emitted OAM beam versus varied q and η with $l = -2$ (here $p = 538$). η_{all} is linearly increased with q or η as seen in Fig. 5(a). In Fig. 5(b), it can be seen that the OAM order purity of $q = 270$ is higher than the others for the same η. The reason is different for the cases of q > 270 and q < 270. Considering the condition of $\eta = 0.01$, according to Eq. (4), when $q = 540$, the intensity of the 270-th and 540-th dipole are < 26% (∼ −5.8 dB) and < 7% (∼ −11.5 dB) of that of the first dipole, respectively. It indicates that the intensity of different dipoles would be more unbalanced for case of $q = 540$. That is to say that the deformation introduced by grating scattering is small for case of $q = 270$. And for other value of η, the conclusion is similar so that C_p of $q = 270$ is higher than that of $q = 540$. When q is less than 270, higher order OAM will also be generated since g could be more than one value. According to Eq. (2), when q is smaller, more values of g could be possible. For $q = 270$, the calculated value of g is a single value of 2, corresponding $l = -2$, but for $q = 180$, there are two possible values ($g = 2$ or 3) so that l could be −2 or 178. Thus C_p of $q = 270$ is higher than $q < 270$. As above discussions, maximum C_p could be achieved with $q = 270$. By considering both the OAM purity and total radiation efficiency, $q = 270$ and $\eta = 0.005$ are chosen to achieve $C_p = \sim 98\%$ and $\eta_{all} = \sim 49\%$. It should be mentioned that only the radiation of upper half-space is considered here so that the maximum value of η_{all} is 50% in theory. That is to say that our optimized $\eta_{all} = 49\%$ is very close to the theoretical upper-limit. For $q = 270$ and $\eta = 0.005$, the intensity distribution and the phase distribution of electric field are also given in Fig. 6 for $l = -4, -2, 2, 4$.

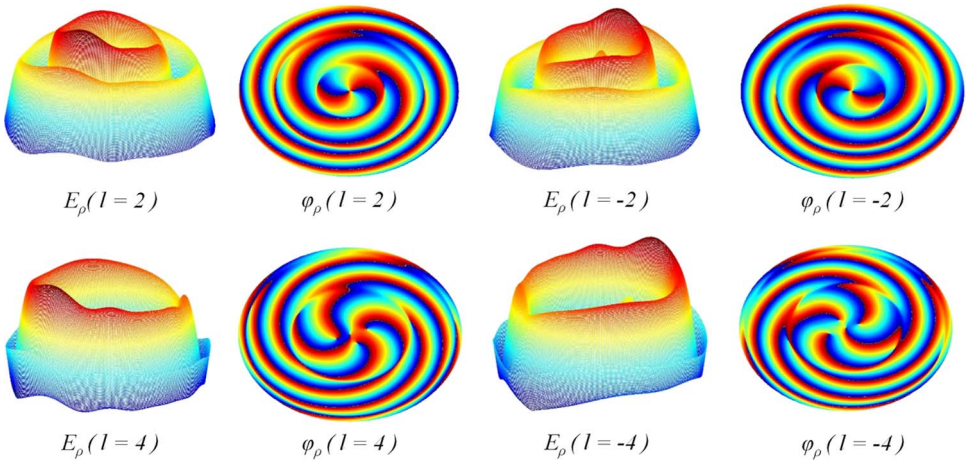

Fig. 6. The intensity distribution and the phase distribution of electric field for $l = -4$, -2, 2, 4 with $q = 270$ and $\eta = 0.005$.

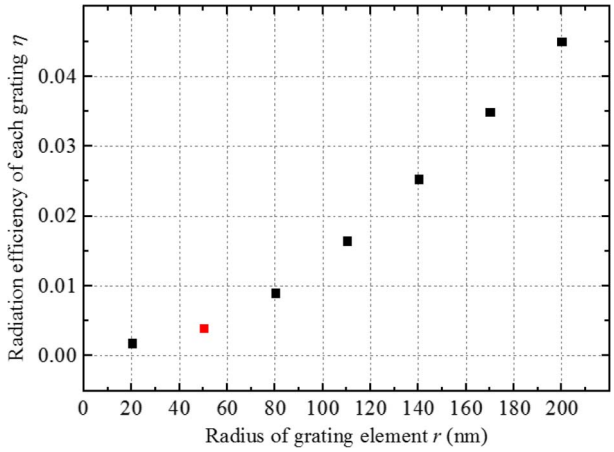

Fig. 7. The radiation efficiency of each grating element (η) corresponding to the radius of the grating element (r).

After q and η are chosen, the structural parameters of OAM beam emitter could be determined in succession. The relation between the radiation efficiency of each grating element (η) and the radius of the grating element (r) is calculated by 3D-FDTD method and shown in Fig. 7. Corresponding to $\eta = 0.005$, the radius is chosen as $r = 50$ nm (the point is marked in red). Taking the value of $q = 270$, $\eta = 0.005$ and attenuation coefficient of $P_l = 1$ dB/cm (both propagation and bending loss are considered), the cross-coupling coefficient is about 0.87 to achieve the critical coupling condition.

Fig. 8 shows the energy ratio between the radially and azimuthally polarized components denoted as W_ρ/W_φ of the designed OAM beam emitter ($q = 270$ and $r = 50$ nm) and C_p for $l = -4 \sim 4$. Here two planes above the emitter of $z = 5\ \mu$m $(z \sim \lambda)$ and $z = 12.5$ mm $(z > 2D^2/\lambda, D = 2R)$ are considered to present the electric field distribution of near-field and far-field. As shown in Fig. 8, the energy ratio W_ρ/W_φ for $z = 5\ \mu$m and $z = 12.5$ mm are calculated as 26 dB $(l = \pm 4) \sim 30$ dB$(l = 0)$ and 11 dB $(l = \pm 4) \sim 27$ dB$(l = 0)$, respectively. When $l = 0$, the energy ratio is more than 27 dB for both near-field and far-field. Although the energy ratio W_ρ/W_φ would be deteriorated along with the distance of light beam propagation, the energy of radially polarized component is still 11 dB higher than that of azimuthal one. According to these results, we believe that the radially polarized OAM beam can be generated by the proposed OAM beam emitter and the OAM order purity C_p could be $\sim$0.98 for $l = -4 \sim 4$.

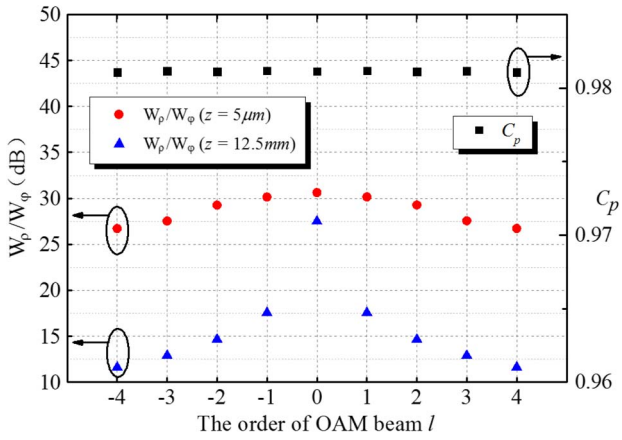

Fig. 8. The results of the OAM beam emitter designed ($q = 270$ and $r = 50$ nm).

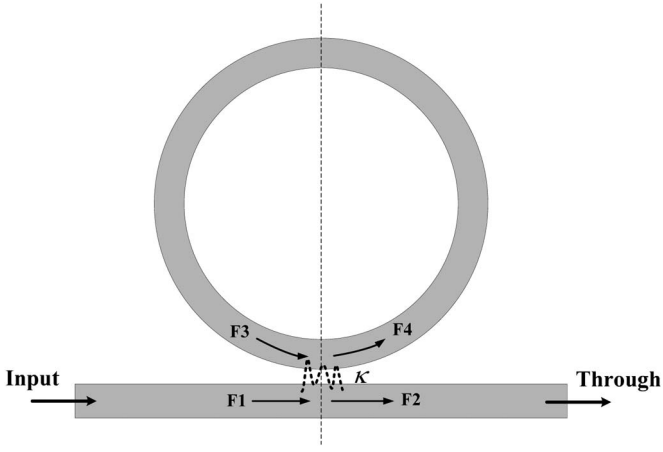

Fig. 9. Scheme of an all-pass ring resonator.

4. Conclusion

A radially polarized OAM beam emitter is proposed on shallow-ridge silicon microring. The number of grating elements q and the radiation efficiency of single grating element η, which are two key structural parameters, are optimized by considering the OAM order purity C_p of OAM beam and the total radiation efficiency η_{all} of the device. According to the calculations, $C_p = \sim 98\%$, $\eta_{all} = \sim 49\%$ are achieved by simulations with $q = 270$ and $\eta = 0.005$. The calculated energy ratio between the far-field radially and azimuthally polarized components is more than 11 dB for the proposed emitter. Here the radius of the microring is 49 μm, the cross-coupling coefficient is about 0.87 and the radius of the grating element is 50 nm.

Appendix

For a ring cavity as shown in Fig. 9, the transmission matrix could be expressed as:

$$\begin{pmatrix} F_4 \\ F_2 \end{pmatrix} = \begin{pmatrix} t & -i\kappa \\ -i\kappa & t \end{pmatrix} \begin{pmatrix} F_3 \\ F_1 \end{pmatrix}. \tag{s1}$$

Here, F_i represents the electric field intensity of corresponding position. t and κ are self- and cross-coupling coefficients and satisfy the relation

$$t^2 + \kappa^2 = 1. \tag{s2}$$

As the gap is designed to satisfy critical coupling, the relation between the field intensity F_4 and the input field intensity F_1 could be obtained as

$$\frac{F_4}{F_1} = -\frac{i}{\sqrt{1-a^2}}. \tag{s3}$$

Here, a represents the single-pass amplitude transmission, and a can be calculated by the radiation efficiency of single grating element (η) and the propagation loss (α) of the waveguide between two adjacent grating elements.

$$a = \left(\sqrt{1-\eta}\cdot(1-\alpha)\right)^q \tag{s4}$$

$$\alpha = \frac{2\pi R}{N}\cdot\left(1-10^{\frac{P_l}{10}}\right) \tag{s5}$$

where P_l is the sum of the propagation loss and bending loss; here, $P_l = 1$ dB/cm, considering the fabrication precision. If we let F_4 equal 1, the total radiation efficiency η_{all} of the OAM beam emitter could be calculated as

$$\begin{aligned}\eta_{all} &= F_4^2\cdot\eta\cdot\sum\left(1+(1-\eta)\cdot(1-\alpha)^2+\cdots+(1-\eta)^{q-1}\cdot(1-\alpha)^{2(q-1)}\right)\\ &= \frac{\eta}{1-(1-\eta)\cdot(1-\alpha)^2}.\end{aligned} \tag{s6}$$

Acknowledgment

The authors would like to thank Dr. W. Zhang, Y. Zhang, and X. Li for their valuable discussions and helpful comments.

References

[1] L. Allen, M. Beijersbergen, R. Spreeuw, and J. Woerdman, "Orbital angular momentum of light and the transformation of Laguerre-Gaussian laser modes," *Phys. Rev. A*, vol. 45, no. 11, pp. 8185–8189, Jun. 1992.
[2] M. Padgett, J. Courtial, and L. Allen, "Light's orbital angular momentum," *Phys. Today*, vol. 57, no. 5, pp. 35–40, 2004.
[3] G. Molina-Terriza, J. P. Torres, and L. Torner, "Twisted photons," *Nature Phys.*, vol. 3, pp. 305–310, 2007.
[4] N. B. Simpson, L. Allen, and M. J. Padgett, "Optical tweezers and optical spanners with Laguerre-Gaussian modes," *J. Mod. Opt.*, vol. 43, no. 12, pp. 2485–2491, Dec. 1996.
[5] H. He, M. Friese, N. Heckenberg, and H. Rubinsztein-Dunlop, "Direct observation of transfer of angular momentum to absorptive particles from a laser beam with a phase singularity," *Phys. Rev. Lett.*, vol. 75, no. 5, pp. 826–829, Jul. 1995.
[6] K. Gahagan and G. Swartzlander, Jr., "Optical vortex trapping of particles," *Opt. Lett.*, vol. 21, no. 11, pp. 827–829, Jun. 1996.
[7] S. Fürhapter, A. Jesacher, S. Bernet, and M. Ritsch-Marte, "Spiral phase contrast imaging in microscopy," *Opt. Exp.*, vol. 13, no. 3, pp. 689–694, Feb. 2005.
[8] J. Lobera and J. Coupland, "Contrast enhancing techniques in digital holographic microscopy," *Meas. Sci. Technol.*, vol. 19, no. 2, p. 025501, Feb. 2008.
[9] A. Mair, A. Vaziri, G. Weihs, and A. Zeilinger, "Entanglement of the orbital angular momentum states of photons," *Nature*, vol. 412, pp. 313–316, 2001.
[10] B. Thidé *et al.,* "Utilization of photon orbital angular momentum in the low-frequency radio domain," *Phys. Rev. Lett.*, vol. 99, no. 8, p. 087701, Aug. 2007.
[11] Z. Bouchal and R. Celechovský, "Mixed vortex states of light as information carriers," *New J. Phys.*, vol. 6, no. 1, p. 131, Oct. 2004.
[12] G. Gibson *et al.,* "Free-space information transfer using light beams carrying orbital angular momentum," *Opt. Exp.*, vol. 12, no. 22, pp. 5448–5456, Nov. 2004.
[13] N. R. Heckenberg, R. McDuff, C. P. Smith, and A. G. White, "Generation of optical phase singularities by computer-generated holograms," *Opt. Lett.*, vol. 17, no. 3, pp. 221–223, Feb. 1992.
[14] M. W. Beijersbergen, R. P. C. Coerwinkel, M. Kristensen, and J. P. Woerdman, "Helical-wavefront laser beams produced with a spiral phaseplate," *Opt. Commun.*, vol. 112, no. 5/6, pp. 321–327, Dec. 1994.

[15] N. Yu *et al.,* "Light propagation with phase discontinuities: Generalized laws of reflection and refraction," *Science*, vol. 334, no. 6054, pp. 333–337, Oct. 2011.
[16] X. Cai *et al.,* "Integrated compact optical vortex beam emitters," *Science*, vol. 338, no. 6105, pp. 363–366, Oct. 2012.
[17] D. Zhang, X. Feng, and Y. Huang, "Encoding and decoding of orbital angular momentum for wireless optical interconnects on chip," *Opt. Exp.*, vol. 20, no. 24, pp. 26 986–26 995, Nov. 2012.
[18] E. Wolf, "Electromagnetic diffraction in opticalsystems. I. An integral representation of the imagefield," in *Proc. R. Soc. London Ser. A*, 1959, vol. 253, pp. 349–357.
[19] B. Richards and E. Wolf, "Electromagnetic diffraction inoptical systems II. Structure of the image field inaplanatic system," in *Proc. R. Soc. London Ser. A*, 1959, vol. 253, pp. 358–379.
[20] D. P. Biss and T. G. Brown, "Cylindrical vector beam focusing through a dielectric interface," *Opt. Exp.*, vol. 9, no. 10, pp. 490–497, Nov. 2001.
[21] T. Kuga *et al.,* "Novel optical trap of atoms with a doughnut beam," *Phys. Rev. Lett.*, vol. 78, no. 25, pp. 4713–4716, Jun. 1997.
[22] K. T. Gahagan and G. A. Swartzlander, Jr., "Simultaneous trapping of low-index and high-index microparticles observed with an optical-vortex trap," *J. Opt. Soc. Amer. B.*, vol. 16, no. 4, pp. 533–537, Apr. 1999.
[23] K. S. Youngworth and T. G. Brown, "Inhomogeneous polarization in scanning optical microscopy," in *Proc. SPIE*, 2000, vol. 3919, pp. 75–85.
[24] J. Zhu, X. Cai, Y. Chen, and S. Yu, "Theoretical model for angular grating-based integrated optical vortex beam emitters," *Opt. Lett.*, vol. 38, no. 8, pp. 1343–1345, Apr. 2013.
[25] A. B. Matsko, A. A. Savchenkov, D. Strekalov, and L. Maleki, "Whispering gallery resonators for studying orbital angular momentum of a photon," *Phys. Rev. Lett.*, vol. 95, no. 14, p. 143 904, Sep. 2005.
[26] P. Dong *et al.,* "Low loss shallow-ridge silicon waveguides," *Opt. Exp.*, vol. 18, no. 14, pp. 14 474–14 479, Jul. 2010.
[27] M. A. Webster, R. M. Pafchek, G. Sukumaran, and T. L. Koch, "Low-loss quasi-planar ridge waveguides formed on thin silicon-on-insulator," *Appl. Phys. Lett.*, vol. 87, no. 23, pp. 231108-1–231108-3, Dec. 2005.
[28] H. Qian, B. D. Markman, and N. C. Giebink, "Vector vortex beam emission from organic semiconductor microlasers," *Appl. Phys. Lett.*, vol. 103, no. 16, pp. 161110-1–161110-5, Oct. 2013.
[29] G. Machavariani *et al.,* "Efficient conversion of a Gaussian beam to a high purity helical beam," *Opt. Commun.*, vol. 209, no. 4–6, pp. 265–271, Aug. 2002.